Gaussian state approximation of quantum many-body scars

Wouter Buijsman* and Yevgeny Bar Lev
Department of Physics, Ben-Gurion University of the Negev, Beer-Sheva 84105, Israel
(Dated: January 8, 2024)

Quantum many-body scars are atypical, highly nonthermal eigenstates embedded in a sea of thermal eigenstates, that have been observed in, for example, kinetically constrained models. These special eigenstates are characterized by a bipartite entanglement entropy that scales as most logarithmically with subsystem size. We use numerical optimization techniques to investigate if quantum many-body scars of the experimentally relevant PXP model are well approximated by Gaussian states. These states are described by a number of parameters that scales quadratically with system size, thereby having a much lower complexity than generic quantum many-body states. We find that while quantum many-body scars away from the center of the spectrum are well approximated by Gaussian states, this is not the case for ergodic eigenstates. This observation suggests that the PXP model is close to certain quadratic parent Hamiltonian, thereby hinting on the origin of quantum many-body scars.

I. INTRODUCTION

Typical isolated quantum many-body systems thermalize under their own internal dynamics [1–3]. Under time evolution, such systems loose information about their initial condition, leading to the emergence of statistical mechanics. Recent times show a keen interest in quantum many-body systems that fall out of this paradigm. By now, several mechanisms leading to the breakdown of thermalization have been identified, among them many-body localization [4–6], quantum many-body scarring [7–9], and Hilbert space fragmentation [10, 11].

Quantum many-body scarring is a form of ergodicity breaking that can be observed, among others, in constrained quantum systems [12]. In contrast to many-body localized systems, quantum many-body scarred systems do not thermalize only when being initialized in certain highly polarized out-of-equilibrium states [13]. These systems show long-living approximate periodic revivals to their initial state, which can be related to a small number of special, highly nonthermal eigenstates embedded in a sea of thermal eigenstates [14]. These special eigenstates are known as quantum many-body scars, in loose analogy to the single-body quantum scars first observed by Heller in 1984 [15]. Quantum many-body scars have attracted tremendous attention both theoretically [7–9] and experimentally [12, 16–19] in recent years. Several models capturing the phenomenon of quantum many-body scarring have been introduced, with the socalled PXP model for a chain of Rydberg atoms being arguably the most paradigmatic example [13, 14, 20].

The origin of quantum many-body scars is part of a timely debate. For a number of models such as the spin-1 XY model, quantum many-body scarred eigenstates can be constructed analytically [9, 21]. For quantum many-body scars without a known exact form, approximate matrix product states can in certain cases be obtained [22–25]. Other works used for example mean-field like methods to approximate quantum many-body scars [26–28], and it has been suggested that they occur due to proximity of the model to to an integrable point [29–31]. Complementary to the approach used in this work (detailed below), it has also been established that the quantum many-body scars of the PXP model admit a description in terms of polyomially many (in system size) low-lying magnon excitations above the ground state [32].

Quantum many body scars have an entanglement entropy which grows at most logarithmically with subsystem size [13, 14]. Since ground states of local quadratic Hamiltontians scale similarly with system size [33], in this work, we consider if quantum many-body scars can be well approximated by ground states of non-interacting systems. These states belong to the a family of Gaussian states (also known as *coherent states*) and are fully described by a number of parameters that scales quadratically with the system size, thereby having a much lower degree of complexity than generic quantum many-body states [34]. Gaussian states have been found to provide an effective description of many-body states in a broad range of settings, for example in the context of the mean-field theory of superconductivity [35], or many-body localization [36–43]. Indications for a Gaussian structure of quantum many-body scars would suggest that the PXP model is close to certain quadratic parent Hamiltonians, hinting on the origin of quantum many-body scars.

In this work, we numerically optimize the parameters of a general non-interacting fermionic system towards a maximum overlap of a symmetrized ground state with a given quantum many-body scar of the PXP model, which is a paradigmatic toy model of quantum many-body scars. Related optimization procedures for a complimentary problem have been found to be fruitful in recent years [44, 45]. We find that Gaussian states provide a good description for the quantum many-body scars away from the center of the spectrum.

The outline of this work is as follows. In Section II, we introduce the model and the properties utilized in the remainder of this work. Section III outlines the ap-

* bwouter@pks.mpg.de

proximation procedure, and in Section IV we present our results. In Section V, we conclude and outline some possible directions for future investigations.

II. MODEL

We consider the PXP model with open boundary conditions,

$$\hat{H}_{\mathrm{PXP}} = \sum_{j=1}^{L-2} \left(\hat{P}_j \, \hat{X}_{j+1} \, \hat{P}_{j+2} \right) + \hat{X}_1 \hat{P}_2 + \hat{P}_{L-1} \hat{X}_L, \quad (1)$$

where $\hat{X}_j = \hat{\sigma}^x_j$ and $\hat{P}_j = \frac{1}{2}\left(1 - \hat{\sigma}^z_j\right)$ with $\hat{\sigma}^x_j$ and $\hat{\sigma}^z_j$ denoting the Pauli x and z operators acting on site j, respectively. Motivated by experiments for which this model results as an effective description [12], up and down spin states are referred to as "ground" and "excited" states, respectively. We consider the experimentally relevant subspace of the Hilbert space that does not contain two neighboring sites in the excited state. Due to the projector terms $\hat{P}_i$, this subspace is decoupled from the rest of the Hilbert space. The Hamiltonian is symmetric with respect to spatial inversion, governed by the operator $\hat{\pi}$, which maps site i to site $L - i + 1$. The Hamiltonian also anti-commutes with the parity operator, $\hat{\mathcal{C}} = \prod_{i=1}^{L} \hat{\sigma}^z_i$, such that if $|\psi_E\rangle$ is an eigenstate of $\hat{H}_{\mathrm{PXP}}$ with eigenvalue E, then $\hat{\mathcal{C}}\,|\psi_E\rangle$ is an eigenstate with energy $-E$. The spectrum is, therefore, symmetric around energy zero and contains an exponentially (in system size) large number of zero-energy eigenstates [46–48]. Since the parity operator has eigenvalues ± 1, any eigenstate of the Hamiltonian can be decomposed as $|\psi_E\rangle = (\hat{P}_+ + \hat{P}_-)|\psi_E\rangle$, where $\hat{P}_\pm$ are the projectors on the corresponding subspaces of $\hat{\mathcal{C}}$. Applying the operator $\hat{\mathcal{C}}$ to this state gives, $\hat{\mathcal{C}}|\psi_E\rangle = (\hat{P}_+ - \hat{P}_-)\,|\psi_E\rangle$, which as mentioned above, corresponds to an eigenstate of energy $-E$. Therefore, for $E \neq 0$, $\langle\psi_E|\hat{\mathcal{C}}|\psi_E\rangle = \langle\psi_E|\hat{P}_+|\psi_E\rangle - \langle\psi_E|\hat{P}_-|\psi_E\rangle = 0$, and we see that $\langle\psi_E|\hat{P}_+|\psi_E\rangle = \langle\psi_E|\hat{P}_-|\psi_E\rangle = 1/2$.

Since we aim to compare eigenstates of a spin model with those of a fermionic model, we express the Hamiltonian of the PXP model in terms of fermionic operators through a Jordan-Wigner transformation,

$$\hat{c}^\dagger_j = e^{i\pi \sum_{k=1}^{j-1} \hat{P}_k} \hat{\sigma}^+_j, \quad (2)$$

$$\hat{c}_j = e^{-i\pi \sum_{k=1}^{j-1} \hat{P}_k} \hat{\sigma}^-_j, \quad (3)$$

$$\hat{c}^\dagger_j \hat{c}_j = \tfrac{1}{2}(1 + \hat{\sigma}^z_j), \quad (4)$$

with $\hat{\sigma}^x_j = \frac{1}{2}(\hat{\sigma}^+_j + \hat{\sigma}^-_j)$. The operators $\hat{c}_j$ and $\hat{c}^\dagger_j$ obey the standard fermionic anti-commutation relations $\{\hat{c}_j, \hat{c}_k\} = \{\hat{c}^\dagger_j, \hat{c}^\dagger_k\} = 0$ and $\{\hat{c}_k, \hat{c}^\dagger_k\} = 1$. We use open boundary conditions to avoid the non-local boundary in the fermionic description which appears for periodic boundary conditions. It is important to note that the mapping to fermionic operators is not unique, and different mappings can potentially give different results.

Quantum many-body scars are eigenstates characterized by an anomalously high overlap with the $\mathbb{Z}_2$-ordered states $|\mathbb{Z}_2\rangle = |\bullet\circ\bullet\circ\cdots\bullet\circ\rangle$ and $|\mathbb{Z}_2'\rangle = |\circ\bullet\circ\bullet\cdots\circ\bullet\rangle$, where $\circ$ and $\bullet$ are pictorial representations of a site in the ground and excited state, respectively [13, 14]. These special eigenstates display a bipartite entanglement entropy that scales at most logarithmically with subsystem size. The null space of the Hamiltonian is also known to host a quantum many-body scar for certain system sizes [13, 22, 49]. As motivated below, we do not consider these zero-energy scars in this work. The quantum-many body scars have almost equal energy separations of $\Omega \approx 1.31$, which only weakly depends of the system size. This results in the appearance of long-lived periodic revivals to the initial state starting from a $\mathbb{Z}_2$-ordered state. The PXP model hosts various additional non-ergodic eigenstates (see, e.g., Ref. [49]), which are sometimes referred to as quantum many-body scars as well. Here, we adapt the more restrictive definition of quantum many-body scars as introduced above. We refer to Ref. [8] for a recent review on the different definitions of quantum many-body scars used in the literature.

III. GAUSSIAN STATE APPROXIMATION

The most general quadratic Hamiltonian with L fermionic modes is given by

$$\hat{H} = \sum_{j,k=1}^{L} \left[A_{jk} \hat{c}^\dagger_j \hat{c}_k + \tfrac{1}{2}\left(B_{jk} \hat{c}^\dagger_j \hat{c}^\dagger_k - B^*_{jk} \hat{c}_j \hat{c}_k \right) \right], \quad (5)$$

where A is Hermitian and B is antisymmetric and the operators $\hat{c}_j$ and $\hat{c}^\dagger_j$ obey the standard fermionic anticommutation relations as introduced above. Fermions are created and annihilated in pairs, meaning that eigenstates can have either an even or an odd number of fermions. Hamiltonian (5) is diagonalized by a Bogoliubov transformation [34, 50, 51],

$$\hat{d}_j = \sum_k \left(U_{jk} \hat{c}_k + V_{jk} \hat{c}^\dagger_k \right) \quad (6)$$

$$\hat{d}^\dagger_j = \sum_k \left(V^*_{jk} \hat{c}^\dagger_k + U^*_{jk} \hat{c}_k \right), \quad (7)$$

where U and V are required to obey $UV^T + VU^T = 0$ and $UU^\dagger + VV^\dagger = 1$ in order for $\hat{d}_j$, $\hat{d}^\dagger_k$ to obey the fermionic anti-commutation relations. The eigenstates of Hamiltonian (5) are thus given by product states in the basis of the quasi-particles created by $\hat{d}^\dagger_i$ on top of a quasi-particle vacuum.

In this work, we focus on the question whether quantum many-body scars can be well approximated by symmetrized ground state of a non-interacting Hamiltonian,

$$|\psi_\pm\rangle = \mathcal{N}\left(|\psi_0\rangle \pm \hat{\pi}|\psi_0\rangle\right). \tag{8}$$

Here $\mathcal{N}$ is a normalization factor, and $|\psi_0\rangle$ is the ground-state of Hamiltonian (5). The states are symmetrized to follow the inversion symmetry of the scars, which results in a better approximation (see Appendix A for details). For quantum many-body scars which are symmetric with respect to inversion we take $|\psi_+\rangle$, and for quantum many-body scars which are antisymmetric we take $|\psi_-\rangle$.

We look for matrices A and B characterizing the quadratic Hamiltonian (5), which give maximal overlap between $|\psi_\pm\rangle$ and a given quantum many-body scar. To compute the overlap, we take the state $|\psi_\pm\rangle$ in the basis where $\hat{n}_j = \hat{c}_j^\dagger \hat{c}_j$ is diagonal, and the quantum many-body scar in the basis where $\hat{\sigma}_j^z$ is diagonal. The PXP Hamiltonian expressed in this basis is a real-valued matrix. Physically, this means that the time-evolution operator is symmetric under time-inversion. Therefore, we lower the computational costs by restricting A and B to be real. Since the quantum many-body scars have considerable overlap with the $\mathbb{Z}_2$ state, for the initial guess of the matrices A and B we use

$$A = \mathrm{diag}\left(\pm 1, 1, -1, 1, \ldots, -1, 1\right) \qquad B = 0, \tag{9}$$

such that the initial ground state of (5) is given by the $\mathbb{Z}_2$ state. The number of fermions in this ground state corresponds to the number of (-1)'s on the main diagonal of A. Since in the fermionic language the parity operator is given by $\hat{\mathcal{C}} = (-1)^{\hat{N}}$, where $\hat{N}$ is the operator counting the number of fermions, a state with an even (odd) number of fermions is an eigenstate of the parity operator with eigenvalue $+1$ (-1). By changing the sign of the first element on the main diagonal of the initial guess for A we can control the evenness of the fermion number and as such the parity of the ground state. We have found empirically that the best optimized output is obtained by changing the sign of the first (or last) diagonal element of A, instead of changing the sign of other diagonal elements of A. Taking the diagonal elements of A as ± 1 in a randomized fashion, such that the initial guess of the ground state is given by a randomly chosen product state, leads to significantly lower optimized overlaps.

For the optimization procedure we use the Limited-Memory Broyden-Fletcher-Goldfarb-Shanno (also known as LM-BFGS) algorithm [52], which we terminate when the gradient of the overlap with respect to the optimization parameters is equal to zero up to numerical precision. In short, this algorithm works in two steps. First, it determines the Hessian of the cost function (here, the overlap) in order to determine the direction in which the increase is maximal. Second, it optimizes the step size in this direction such that the increase is at its maximum. For small system sizes, we have tested the performance of all optimization algorithms implemented in the Python SciPy package [53]. We empirically observed that this algorithm provides optimal results in terms of the optimized overlaps. We remark that it is generically impossible to analytically find the optimal parameters of a Gaussian state approximating a given many-body state [54]. As the optimization algorithm (like all numerical optimization algorithms) searches for local maxima, it is important to ensure the initial guess to be as close as possible to the desired result. One could alternatively choose A and B such that the ground state of $\hat{H}$ is given by the product state that has the highest overlap with the quantum many-body scar under consideration. For the quantum many-body scars closer to the center of the spectrum, this is not always the $\mathbb{Z}_2$ state. For this, we find qualitatively similar results. Initializing A and B with random elements (subject to the symmetry constraints) gives, as expected, very low optimized overlaps.

We consider relatively modest system sizes due to the high computational costs of the optimization procedure. Typically, optimization requires several thousands, or with outliers, several tens of thousands evaluations of the overlap. For each such overlap the *many-body* ground-state of the quadratic system has to be re-calculated. We note that, while the single-particle states of a quadratic model can be computed in time polynomially with the system size, the computation of the *many-body* ground state scales exponentially with the system size. We note in passing, that the outlined procedure does *not* typically correspond to the calculation of the natural orbitals from the diagonalization of the single-particle density matrix. In fact, it is known that a ground state constructed in the basis of natural orbitals produces optimal results only for states with two fermions [54, 55].

IV. RESULTS

Since the quadratic Hamiltonian (5) conserves the parity of the number of fermions, we have to approximate the projections of the scars onto different parity sectors, $\hat{P}_\pm|\psi_{\mathrm{scar}}\rangle$, separately. We note, that for system sizes dividable by 4, the $\mathbb{Z}_2$ state lies in the positive parity sector and in the negative parity sector otherwise. On the other hand, as shown in Section II, all eigenstates of the PXP model (with nonzero eigenvalue), including the quantum many-body scars, have the same overlap 1/2 with both sectors. We denote by $|\psi_{\mathrm{init}}\rangle$ the symmetrized ground state of Hamiltonian (5) which corresponds to the initial choice of matrices A and B according to (9). The resulting optimized symmetrized state will be denoted by $|\psi_{\mathrm{opt}}\rangle$. For convenience, in what follows we focus on the quantity $4|\langle\psi_{\mathrm{opt}}|\hat{P}_\pm|\psi_{\mathrm{scar}}\rangle|^2$, which is bounded from above by unity, since $\langle\psi_{\mathrm{scar}}|\hat{P}_\pm|\psi_{\mathrm{scar}}\rangle = 1/2$ (see Section II). We focus only on scars with positive energies, $E_{\mathrm{scar}} > 0$, since the spectrum of the PXP model is symmetric around zero . We do not consider quantum many-body scars at zero energy, since quantum many-body scars are not uniquely defined due to the numerous

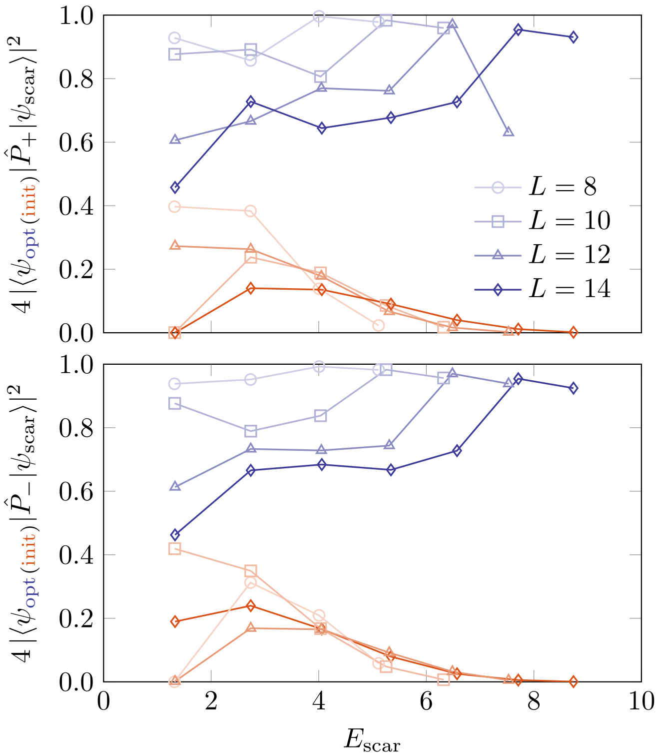

FIG. 1. Blue lines (upper sets of curves) show the optimized overlaps $4|\langle\psi_{\rm opt}|\hat{P}_+|\psi_{\rm scar}\rangle|^2$(upper panel) and $4|\langle\psi_{\rm opt}|\hat{P}_-|\psi_{\rm scar}\rangle|^2$ (lower panel) for several system sizes as a function of the energy of the quantum many-body scars. Red lines (lower sets of curves) show the overlap $4|\langle\psi_{\rm init}|\hat{P}_+|\psi_{\rm scar}\rangle|^2$ (upper panel) and $4|\langle\psi_{\rm init}|\hat{P}_-|\psi_{\rm scar}\rangle|^2$ (lower panel). The largest possible overlap with this normalization is unity.

degeneracy at zero energy.

Fig. 1 shows the initial $4|\langle\psi_{\rm init}|\hat{P}_\pm|\psi_{\rm scar}\rangle|^2$ and optimized overlaps $4|\langle\psi_{\rm opt}|\hat{P}_\pm|\psi_{\rm scar}\rangle|^2$ for system sizes $L=8$ to $L=14$ as a function of the energies of the scars, $E_{\rm scar}$. We observe that the optimized overlap is close to unity for the two quantum many-body scars closest to the edge of the spectrum. In fact, the highest-energy scars are the highest excited eigenstates (or, equivalently, the ground states). We also note that the optimization leads to a significant improvement of the overlap for quantum many-body scars away from the center of the spectrum, as can be seen by comparing to the overlap with the initial guess, $|\psi_{\rm init}\rangle = (|\mathbb{Z}_2\rangle \pm |\mathbb{Z}_2'\rangle)/\sqrt{2}$. In Appendix B, we show that significantly lower overlaps, in particular at larger system sizes, are obtained for non-scarred (thermal) eigenstates. We note in passing, that although the optimized states are not confined to the constrained Hilbert space of the PXP model by construction, the high overlap implies that the optimized states almost fully reside there.

Quantum many-body scars distinguish themselves from other types of non-ergodic many-body states by their anomalously high overlap with the $|\mathbb{Z}_2\rangle$ and $|\mathbb{Z}_2'\rangle$

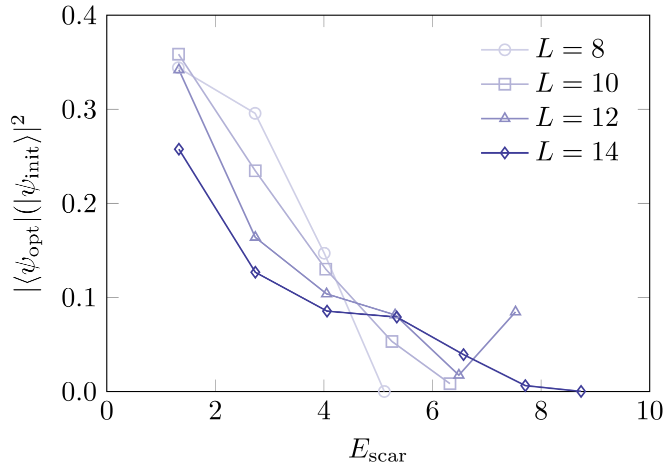

FIG. 2. The overlap $|\langle\psi_{\rm opt}|\psi_{\rm init}\rangle|^2$ as a function of the energy of the quantum many-body scars at several system sizes.

states. This can be seen at the lower (red) set of lines in Fig. 1, which shows the overlap, $4|\langle\psi_{\rm init}|\hat{P}_+|\psi_{\rm scar}\rangle|^2$, where $|\psi_{\rm init}\rangle = (|\mathbb{Z}_2\rangle \pm |\mathbb{Z}_2'\rangle)/\sqrt{2}$. In Fig. 2, we see that also the optimized state has a qualitatively similar overlap with the $|\mathbb{Z}_2\rangle$ and $|\mathbb{Z}_2'\rangle$ states, by plotting $|\langle\psi_{\rm init}|\psi_{\rm opt}\rangle|^2$ as a function of the energy of the quantum many-body scars for the system sizes considered above. It is interesting to note that at the edges of the spectrum where the approximation of the scars is the best, the optimized and initial states are almost orthogonal to each other.

The structure of the optimized matrices A and B could provide insight on the structure of the quantum many-body scars. Fig. 3 shows color plots of the optimized matrices for the scar with the second-highest (the highest-energy scar is the ground state) energy at system size $L=14$. The optimized Hamiltonian exhibits a notion of locality, reflected in the band-like structure. This observation is presumably related to the low-entanglement property of the quantum many-body scars. We observe a checkerboard-pattern of the matrices A and B that suggests a translational invariance for translations over two sites, instead of "full" translational invariance. This does not appear to be surprising given the fact that our trail wavefunctions [Eq. 8] break the translational invariance of the matrices A and B. We found that enforcing translation invariance in the trial wavefunctions yields considerably lower overlaps. This provides a hint that the exact quantum many-body scars are superpositions of states invariant under translations by two sites.

V. CONCLUSIONS AND OUTLOOK

Quantum many-body scars are states with low entanglement embedded in ergodic eigenstates. In this work, we have studied to what extent quantum many-body scars in the PXP model can be described by inversion

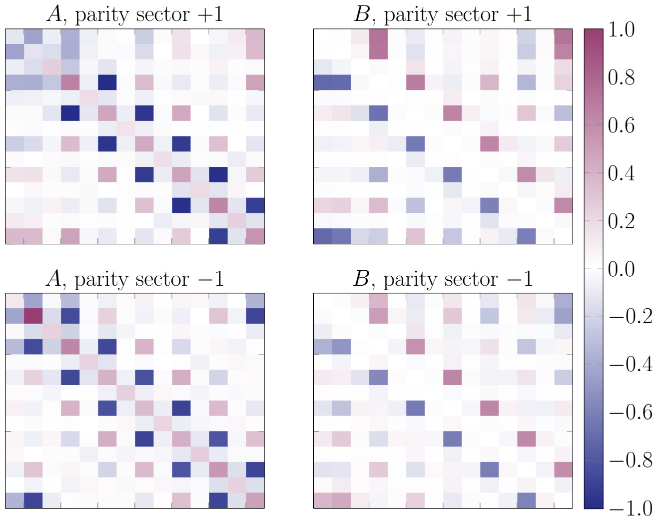

FIG. 3. Color plots of the matrices A (left) and B (right) of the quadratic Hamiltonian (5), whose ground-state has the largest overlap with the scar with the second-highest energy for $L = 14$. The top panels correspond to optimization with respect to $\hat{P}_+ |\psi_{\text{scar}}\rangle$ and the bottom panels with respect to $\hat{P}_- |\psi_{\text{scar}}\rangle$. The scale has been chosen such that the largest absolute value is unity.

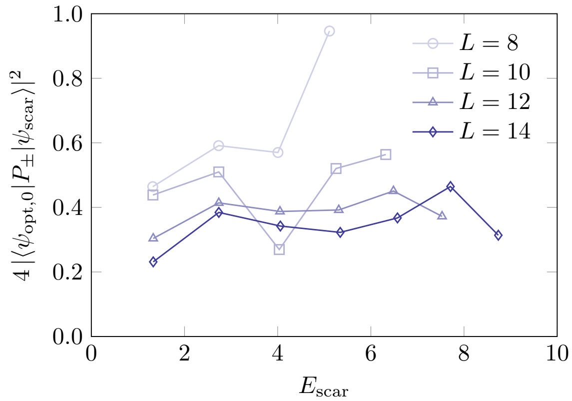

FIG. 4. The optimized overlaps $4|\langle\psi_{\text{scar}}|\hat{P}_\pm|\psi_{\text{opt},0}\rangle|^2$ for several system sizes as a function of the energy of the quantum many-body scars. The sign of the projector $P_\pm$ is chosen such that it projects on to the parity sector containing the $\mathbb{Z}_2$ state. The largest possible overlap with this normalization is unity.

symmetrized Gaussian states, which corresponds to a ground state of a quadratic Hamiltonian with no particle number conservation. This is not guaranteed *a-priori*, since not all low-entangled states are Gaussian. We numerically optimized the parameters of the most general quadratic fermionic Hamiltonian such that the ground state has maximal overlap with the quantum many-body scar under consideration. We found that quantum many-body scars away from the center of the spectrum can be well described by states of this form. This holds in particular for the highest (or equivalently, lowest) energy quantum many-body scar. We also showed, that the optimal quadratic Hamiltonian is local, has a non-negligible pairing and is translationally invariant only every *two* sites. In fact, enforcing full translation invariance in the optimization procedure, provides considerably lower overlaps (not shown). Since entanglement entropy of ground-states of local quadratic Hamiltonians scales logarithmically with the system size [33], our result suggests that similar scaling will hold also for quantum many-body scars, at least not too close to the center of the spectrum. It is important to note, that the optimization of ergodic, non-scarred, eigenstates, leads to very poor results, indicating that while the scarred states have Gaussian structure, this is not the case for the ergodic states.

In this work, we have used a distinct quadratic Hamiltonian for each quantum many-body scar. In future studies, it would be interesting to see if a single optimal quadratic Hamiltonian can be used to reasonably capture the structure of each of the scars, as also to understand the origin of such an effective single-particle description. A related open question is whether multiple distinct parent Hamiltonians can be found for a given quantum many-body scar. This question is relevant, in particular, when aiming to unify the various approximation schemes that have been proposed in the literature. It would be also interesting to investigate further if similar results can be obtained for other quantum many-body scarred models.

ACKNOWLEDGMENTS

This research was supported by a grant from the United States-Israel Binational Foundation (BSF, Grant No. 2019644), Jerusalem, Israel, and the United States National Science Foundation (NSF, Grant No. DMR-1936006), and by the Israel Science Foundation (grants No. 527/19 and 218/19). WB acknowledges support from the Kreitman School of Advanced Graduate Studies at Ben-Gurion University.

Appendix A: Optimization results for non-symmetrized Gaussian states

Here, we study the overlap of quantum many-body scars with optimized Gaussian states, here denoted by $|\psi_{\text{opt},0}\rangle$, instead of the symmetrized version $|\psi_{\text{opt}}\rangle$ [see (8)]. As this investigation is only for illustrative purposes, we restrict the analysis to optimization with respect to the parity sector containing the $\mathbb{Z}_2$ state, which is arguably physically the most interesting. Fig. 4 shows the optimized overlaps as a function of the energy of the quantum many-body scar for several system sizes. Comparing the results with those shown in Fig. 1, we observe a substantially lower overlap, which highlights the importance of symmetrization.

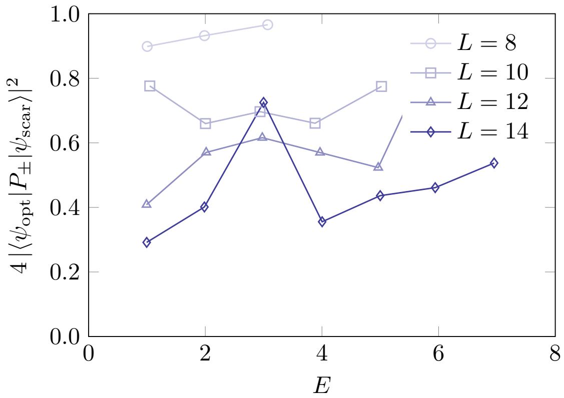

FIG. 5. The optimized overlaps $4|\langle\psi_{\rm scar}|\hat{P}_{\pm}|\psi_{\rm opt}\rangle|^2$ for several system sizes as a function of the energy for thermal eigenstates. See the main text for the choice of the eigenstates. The sign of the projector $P_{\pm}$ is chosen such that it projects on to the parity sector containing the $\mathbb{Z}_2$ state. The largest possible overlap with this normalization is unity.

Appendix B: Optimization results for thermal eigenstates

Here, we study the overlap of thermal states with optimized (symmetrized) Gaussian states. We restrict the analysis to optimization with respect to the parity sector containing the $\mathbb{Z}_2$ state, which is arguably physically the most interesting. For each system size, we consider the eigenstates with energies closest to integers. If such an eigenstatate is a quantum many-body scar, we take the eigenstate with the second-closest energy. Fig. 5 shows the results. For $L = 8$ we observe similar overlaps for thermal and quantum many-body scarred eigenstates (cf. Fig. 1). We observe that the overlap for thermal states decreases rapidly with increasing system size, indicating that thermal and quantum many-body scarred eigenstates have qualitatively different structures.

[1] F. Borgonovi, F. M. Izrailev, L. F. Santos, and V. G. Zelevinsky, Quantum chaos and thermalization in isolated systems of interacting particles, Phys. Rep. **626**, 1 (2016).

[2] L. D'Alessio, L. Kafri, A. Polkovnikov, and M. Rigol, From quantum chaos and eigenstate thermalization to statistical mechanics and thermodynamics, Adv. Phys. **65**, 239 (2016).

[3] J. M. Deutsch, Eigenstate thermalization hypothesis, Rep. Prog. Phys. **81**, 082001 (2018).

[4] D. M. Basko, I. L. Aleiner, and B. L. Altshuler, On the problem of many-body localization, in *Problems of Condensed Matter Physics: Quantum coherence phenomena in electron-hole and coupled matter-light systems*, edited by A. L. Ivanov and S. G. Tikhodeev (Oxford University Press, Oxford, 2007).

[5] R. Nandkishore and D. A. Huse, Many-Body Localization and Thermalization in Quantum Statistical Mechanics, Annu. Rev. Condens. Matter Phys. **6**, 15 (2015).

[6] D. A. Abanin, E. Altman, I. Bloch, and M. Serbyn, Colloquium: Many-body localization, thermalization, and entanglement, Rev. Mod. Phys. **91**, 021001 (2019).

[7] M. Serbyn, D. A. Abanin, and Z. Papić, Quantum many-body scars and weak breaking of ergodicity, Nat. Phys **17**, 675 (2021).

[8] Z. Papić, Weak Ergodicity Breaking Through the Lens of Quantum Entanglement, in *Entanglement in Spin Chains: From Theory to Quantum Technology Applications*, edited by A. Bayat, S. Bose, and H. Johannesson (Springer, Cham, 2022).

[9] A. Moudgalya, B. Andrei Bernevig, and N. Regnault, Quantum many-body scars and Hilbert space fragmentation: a review of exact results, Rep. Prog. Phys. **85**, 086501 (2022).

[10] P. Sala, T. Rakovszky, R. Verresen, M. Knap, and F. Pollmann, Ergodicity Breaking Arising from Hilbert Space Fragmentation in Dipole-Conserving Hamiltonians, Phys. Rev. X , 011047 (2020).

[11] V. Khemani, M. Hermele, and R. Nandkishore, Localization from Hilbert space shattering: From theory to physical realizations, Phys. Rev. B **101**, 174204 (2020).

[12] H. Bernien, S. Schwartz, A. Keesling, H. Levine, A. Omran, H. Pichler, S. Choi, A. S. Zibrov, M. Endres, M. Greiner, V. Vuletić, and M. D. Lukin, Probing many-body dynamics on a 51-atom quantum simulator, Nature **551**, 579 (2017).

[13] C. J. Turner, A. A. Michailidis, A. A. Abanin, M. Serbyn, and Z. Papić, Weak ergodicity breaking from quantum many-body scars, Nat. Phys. **14**, 745 (2018).

[14] C. J. Turner, A. A. Michailidis, D. A. Abanin, M. Serbyn, and Z. Papić, Quantum scarred eigenstates in a Rydberg atom chain: Entanglement, breakdown of thermalization, and stability to perturbations, Phys. Rev. B **98**, 155134 (2018).

[15] E. J. Heller, Bound-State Eigenfunctions of Classically Chaotic Hamiltonian Systems: Scars of Periodic Orbits, Phys. Rev. Lett. **53**, 1515 (1984).

[16] D. Bluvstein, A. Omran, H. Levine, A. Keesling, G. Semeghini, S. Ebadi, T. T. Wang, A. A. Michailidis, N. Maskara, W. W. Ho, S. Choi, M. Serbyn, M. Greiner, V. Vuletić, and M. D. Lukin, Controlling quantum many-body dynamics in driven Rydberg atom arrays, Science **371**, 1355 (2021).

[17] D. Bluvstein, H. Levine, G. Semeghini, T. T. Wang, S. Ebadi, M. Kalinowski, A. Keesling, N. Maskara, H. Pichler, V. Greiner, M. Vuletić, and M. D. Lukin, A quantum processor based on coherent transport of entangled atom arrays, Nature **604**, 451 (2022).

[18] G.-X. Su, H. Sun, A. Hudomal, J.-Y. Desaules, Z.-Y. Zhou, B. Yang, J. C. Halimeh, Z.-S. Yuan, Z. Papić, and J.-W. Pan, Observation of many-body scarring in a Bose-Hubbard quantum simulator, Phys. Rev. Res. **5**, 023010 (2023).

[19] P. Zhang, H. Dong, Y. Gao, L. Zhao, J. Hao, J.-Y. Desaules, Q. Guo, J. Chen, J. Deng, B. Liu, W. Ren, Y. Yao, X. Zhang, S. Xu, K. Wang, F. Jin, X. Zhu, B. Zhang,

H. Li, C. Song, Z. Wang, F. Liu, L. Papić, Z. andYing, H. Wang, and Y.-C. Lai, Many-body Hilbert space scarring on a superconducting processor, Nature Phys. **19**, 120 (2023).

[20] I. Lesanovsky and H. Katsura, Interacting Fibonacci anyons in a Rydberg gas, Phys. Rev. A **86**, 041601 (2012).

[21] A. Chandran, T. Iadecola, V. Khemani, and R. Moessner, Quantum Many-Body Scars: A Quasiparticle Perspective, Annu. Rev. Condens. Matter Phys. **14**, 443 (2023).

[22] C.-J. Lin and O. I. Motrunich, Exact Quantum Many-Body Scar States in the Rydberg-Blockaded Atom Chain, Phys. Rev. Lett. **122**, 173401 (2019).

[23] W. W. Ho, S. Choi, H. Pichler, and M. D. Lukin, Periodic Orbits, Entanglement, and Quantum Many-Body Scars in Constrained Models: Matrix Product State Approach, Phys. Rev. Lett. **122**, 040603 (2019).

[24] S. Chattopadhyay, H. Pichler, M. D. Lukin, and W. W. Ho, Quantum many-body scars from virtual entangled pairs, Phys. Rev. B **101**, 174308 (2020).

[25] S.-Y. Zhang, D. Yuan, T. Iadecola, S. Xu, and D.-L. Deng, Extracting Quantum Many-Body Scarred Eigenstates with Matrix Product States, Phys. Rev. Lett. **131**, 020402 (2023).

[26] C. J. Turner, J.-Y. Desaules, K. Bull, and Z. Papić, Correspondence Principle for Many-Body Scars in Ultracold Rydberg Atoms, Phys. Rev. X **11**, 021021 (2021).

[27] K. Omiya and M. Müller, Quantum many-body scars in bipartite Rydberg arrays originating from hidden projector embedding, Phys. Rev. A **107**, 023318 (2023).

[28] Q. Hummel, K. Richter, and P. Schlagheck, Genuine Many-Body Quantum Scars along Unstable Modes in Bose-Hubbard Systems, Phys. Rev. Lett. **130**, 250402 (2023).

[29] V. Khemani, C. R. Laumann, and A. Chandran, Signatures of integrability in the dynamics of Rydberg-blockaded chains, Phys. Rev. B **99**, 161101 (2019).

[30] F. M. Surace, P. P. Mazza, G. Giudici, A. Lerose, A. Gambassi, and M. Dalmonte, Lattice Gauge Theories and String Dynamics in Rydberg Atom Quantum Simulators, Phys. Rev. X **10**, 021041 (2020).

[31] L. Pan and H. Zhai, Composite spin approach to the blockade effect in Rydberg atom arrays, Phys. Rev. Res. **4**, L032037 (2022).

[32] T. Iadecola, M. Schecter, and S. Xu, Quantum many-body scars from magnon condensation, Phys. Rev. B **100**, 184312 (2019).

[33] P. Calabrese and J. Cardy, Entanglement entropy and quantum field theory, J. Stat. Mech.: Theory Exp. **2004**, 06002.

[34] P. Perelomov, *Generalized Coherent States and Their Applications* (Springer-Verlag, Berlin, 1986).

[35] Y. Asano, *Andreev Reflection in Superconducting Junctions* (Springer, New York, 2021) Chap. 3.

[36] S. Bera, H. Schomerus, F. Heidrich-Meisner, and J. H. Bardarson, Many-Body Localization Characterized from a One-Particle Perspective, Phys. Rev. Lett. **115**, 046603 (2015).

[37] S. Bera, T. Martynec, H. Schomerus, F. Heidrich-Meisner, and J. H. Bardarson, One-particle density matrix characterization of many-body localization, Ann. Phys. (Berlin, Ger.) **529**, 1600356 (2017).

[38] T. L. M. Lezama, S. Bera, H. Schomerus, F. Heidrich-Meisner, and J. H. Bardarson, One-particle density matrix occupation spectrum of many-body localized states after a global quench, Phys. Rev. B **96**, 060202 (2017).

[39] B. Villalonga, X. Yu, D. J. Luitz, and B. K. Clark, Exploring one-particle orbitals in large many-body localized systems, Phys. Rev. B **97**, 104406 (2018).

[40] W. Buijsman, V. Gritsev, and V. Cheianov, Many-body localization in the Fock space of natural orbitals, SciPost Phys. **4**, 038 (2018).

[41] M. Hopjan and F. Heidrich-Meisner, Many-body localization from a one-particle perspective in the disordered one-dimensional Bose-Hubbard model, Phys. Rev. A **101**, 063617 (2020).

[42] T. Orito and K.-I. Imura, Multifractality and Fock-space localization in many-body localized states: One-particle density matrix perspective, Phys. Rev. B **103**, 214206 (2021).

[43] M. Hopjan, F. Heidrich-Meisner, and V. Alba, Scaling properties of a spatial one-particle density-matrix entropy in many-body localized systems, Phys. Rev. B **104**, 035129 (2021).

[44] C. J. Turner, K. Meichanetzidis, Z. Papić, and J. K. Pachos, Optimal free description of many-body theories, Nat. Phys. **14**, 745 (2018).

[45] J. K. Pachos and C. Vlachou, Quantifying fermionic interactions from the violation of wick's theorem, Quantum **6**, 840 (2022).

[46] M. Schecter and T. Iadecola, Many-body spectral reflection symmetry and protected infinite-temperature degeneracy, Phys. Rev. B **98**, 035139 (2018).

[47] V. Karle, M. Serbyn, and A. A. Michailidis, Area-Law Entangled Eigenstates from Nullspaces of Local Hamiltonians, Phys. Rev. Lett. **127**, 060602 (2021).

[48] W. Buijsman, Number of zero-energy eigenstates in the PXP model, Phys. Rev. B **106**, 045104 (2022).

[49] F. M. Surace, M. Votto, E. G. Lazo, A. Silva, M. Dalmonte, and G. Giudici, Exact many-body scars and their stability in constrained quantum chains, Phys. Rev. B **103**, 104302 (2021).

[50] N. N. Bogoliubov, On the theory of superfluidity, J. Phys. (USSR) **11**, 23 (1947).

[51] E. Lieb, T. Schultz, and D. Mattis, Two soluble models of an antiferromagnetic chain, Ann. Phys. **16**, 407 (1961).

[52] H. A. Byrd, P. Lu, J. Nocedal, and C. Zhu, A Limited Memory Algorithm for Bound Constrained Optimization, SIAM J. Sci. Comput. **16**, 1190 (1995).

[53] P. Virtanen, R. Gommers, T. E. Oliphant, M. Haberland, T. Reddy, D. Cournapeau, E. Burovski, P. Peterson, W. Weckesser, J. Bright, S. J. van der Walt, M. Brett, J. Wilson, K. J. Millman, N. Mayorov, A. R. J. Nelson, E. Jones, R. Kern, E. Larson, C. J. Carey, I. Polat, Y. Feng, E. W. Moore, J. VanderPlas, D. Laxalde, J. Perktold, R. Cimrman, I. Henriksen, E. A. Quintero, C. R. Harris, A. M. Archibald, A. H. Ribeiro, F. Pedregosa, P. van Mulbregt, and S. . Contributors, SciPy 1.0: Fundamental algorithms for scientific computing in Python, Nature Methods **17**, 261 (2020).

[54] J. M. Zhang and N. J. Mauser, Optimal Slater-determinant approximation of fermionic wave functions, Phys. Rev. A **94**, 032513 (2016).

[55] Y. A. Aoto and M. F. da Silva, Calculating the distance from an electronic wave function to the manifold of Slater determinants through the geometry of Grassmannians, Phys. Rev. A **102**, 052803 (2020).